CDF Note 9284 v1.0

Search for Higgs Bosons Produced in Association with b-Quarks

The CDF Collaboration

URL http://www-cdf.fnal.gov

(Dated: April 7, 2008)

We present a search for neutral Higgs bosons decaying into $b\bar{b}$, produced in association with b-quarks in $p\bar{p}$ collisions. This process could be observable in supersymmetric models with high values of $\tan\beta$. We search for an enhancment in the mass of the two lead jets in triply b-tagged events, using 1.9 fb^{-1} of data collected with the CDF II detector at the Fermilab Tevatron collider. The dijet mass spectrum of the heavy flavor multi-jet background is derived from double-tagged data in a manner that accounts for tagging biases and kinematic differences introduced by the addition of the third tag. We set mass-dependent limits on $\sigma \times BR$ and $\tan\beta$ in MSSM models.

Preliminary Results for Winter 2008 Conferences

FIG. 1: MSSM Higgs cross sections for various production modes at $\tan\beta = 40$ in the m_h^{max} scenario, from the TeV4LHC Working Group [2].

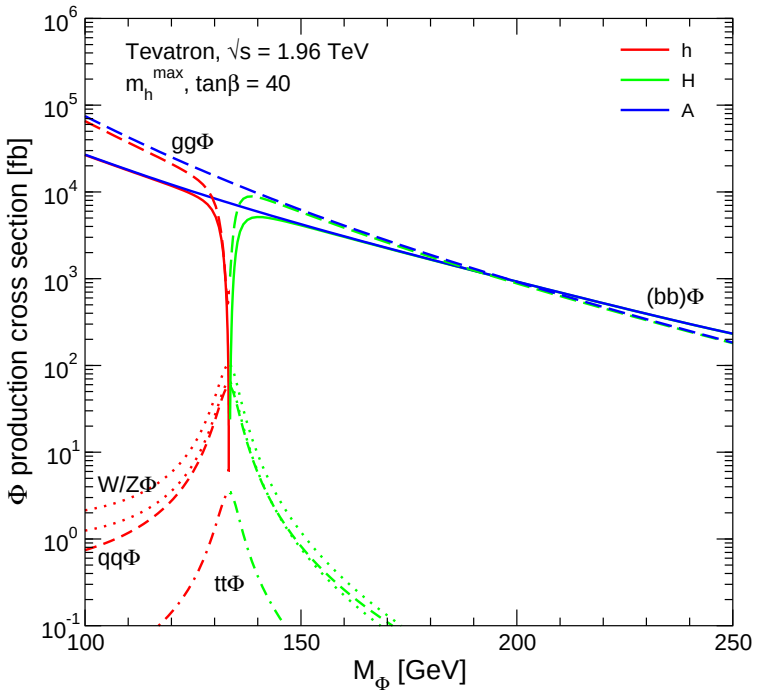

I. INTRODUCTION

The production rate of light Higgs bosons in association with b-quarks can be significantly enhanced in supersymmetric extensions of the standard model. This occurs for large values of $\tan\beta$, the ratio of the Higgs coupling to down-type versus up-type quarks. Figure 1 shows the cross section expected for $\tan\beta = 40$ in the m_h^{max} benchmark scenario [1], from the TeV4LHC Working Group [2]. The cross section for $(bb)\Phi$ is in the 10 pb range, which could potentially be observable at the Tevatron. Also interesting is that at large $\tan\beta$ the pseudoscalar A becomes degenerate with either the light (h) or heavy (H) scalar, giving an effective factor of two enhancement to the cross section.

The cross sections shown in Figure 1 are for inclusive production [3], however only the case where at least one of the b's accompanying the Higgs is at high p_T is relevant to these results, since we will require that it be b-tagged. As shown in Figure 2, cross section calculations are available for this case as well [4, 5, 6, 7], allowing for the interpretation of the results of the search described in this note.

Results for the Higgs+1b process in the case of Higgs decays to $b\bar{b}$ have been obtained by DØ [8, 9], and for inclusive Higgs production in the $\tau\tau$ decay mode by CDF [10, 11] and DØ [12, 13, 14].

In this analysis we search for Higgs decays into $b\bar{b}$, accompanied by an additional high-p_T b, giving an event signature of at least three b-jets. We study the dijet mass spectrum of the two leading jets in three-jet events with all three jets identified as b-jet candidates

FIG. 2: MSSM Higgs cross sections at $\tan\beta = 40$ as a function of the number of high-p_T b quarks accompanying the Higgs (taken from Ref. [5]).

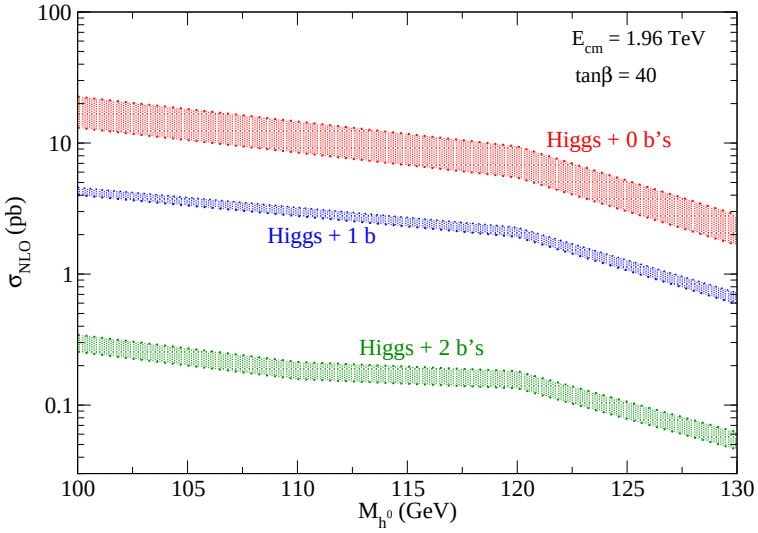

FIG. 3: The tag mass m^{tag} for different jet flavors.

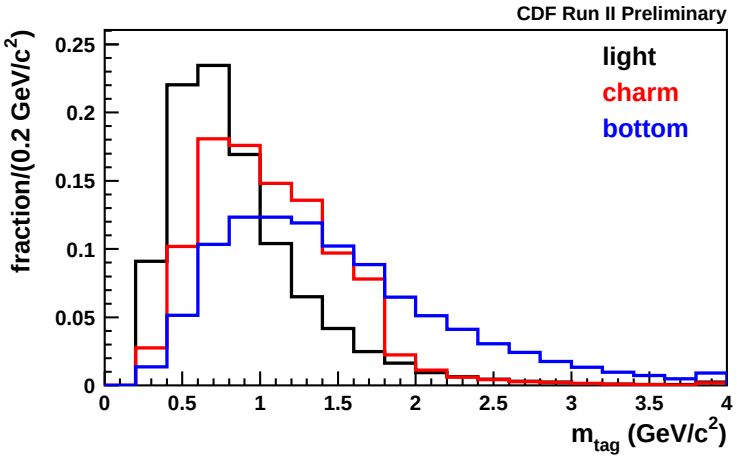

using a displaced vertex algorithm [15]. We use the dijet mass of the two leading jets in the events m_{12} to separate Higgs signal from background events. We also define a quantity $x_{tags}(m_1^{tag} + m_2^{tag}, m_3^{tag})$, where m_i^{tag} is the mass of the tracks forming the displaced vertex in jet 1, 2, or 3. The m^{tag} are sensitive to the flavor of the jet as shown in Figure 3.

The x_{tags} variable is defined as

$$x_{tags} = \begin{cases} \max(m_3^{tag}, 2.99) & : \quad m_1^{tag} + m_2^{tag} < 2 \\ \max(m_3^{tag}, 2.99) + 3 & : \quad 2 \leq m_1^{tag} + m_2^{tag} < 4 \\ \max(m_3^{tag}, 2.99) + 6 & : \quad m_1^{tag} + m_2^{tag} \geq 4 \end{cases} \tag{1}$$

FIG. 4: Illustration of the x_{tags} definition.

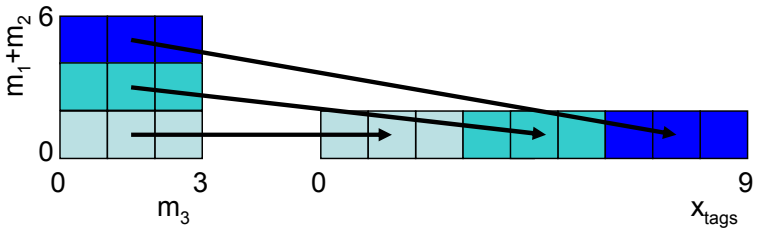

where $\max(a, b)$ returns the maximum of a and b, and all quantities are in units of GeV/c^2. The net effect is to unstack a two-dimensional histogram of $m_1^{tag} + m_2^{tag}$ versus m_3^{tag} into the one-dimensional variable x_{tags}, as illustrated in Figure 4.

II. DATA SAMPLE & EVENT SELECTION

This analysis is based on an integrated luminosity of 1.9 fb^{-1} collected with the CDF II detector [16] between February 2002 and May 2007. The data are collected on a trigger requiring two central energy clusters with $E_T > 15$ GeV and a third cluster with $E_T > 10$ GeV. The 15 GeV clusters are each required to match in ϕ to a track with $p_T > 2$ GeV/c and impact parameter $|d_0| > 120$ μm, reconstructed using the Level2 silicon vertex tracker system.

The offline selection requires three jets with $E_T > 20$ GeV and detector rapidity $|\eta| < 2$. The jets are reconstructed using a cone algorithm with radius $\delta R = \sqrt{\delta\phi^2 + \delta\eta^2} < 0.7$, and are corrected for calorimeter response and multiple interactions so that the energy scale mirrors the total p_T of all particles within the jet cone. The two leading jets in the event must match to the 15 GeV energy clusters and displaced tracks in the Level2 trigger selection, and the third jet is require to match the additional 10 GeV cluster. All three of the jets must be tagged as b-jets using the SECVTX algorithm [15], which searches for displaced b-decay vertices using the tracks within the jet cone. We also select an auxiliary sample with no SECVTX tag requirement on the third jet which is used for constructing background estimates.

To compute the efficiency of this selection, the cross section being measured must be precisely defined. We use the MCFM program to calculate the cross section for $bg \to H + b_{jet}$ which corresponds to the three-b-jet event selection. The notation b_{jet} refers to the clustering of final-state partons performed by MCFM. If there is a gluon in the final state along with the outgoing b quark (MCFM does not decay the Higgs) and they are within $\delta R < 0.4$ of each other, MCFM will combine them into a "jet", otherwise the b quark alone serves as the jet. This b-jet is the object upon which the kinematic cuts can be applied.

We calculate the cross section for $H + b_{jet}$ in the SM, requiring $p_T > 15$ GeV/c and $|\eta| < 2$ for the b_{jet} to match the b-tagging acceptance of the SECVTX algorithm. We used CTEQ6.5M [17] parton distribution functions and set the renormalization and factorization scales to $\mu_R = \mu_F = (2m_b + m_H)/4$ as suggested in Refs. [7, 18]. The cross section obtained as a function of m_H is shown in Figure 5.

FIG. 5: SM cross section for $bg \to H + b_{jet}$ calculated with MCFM.

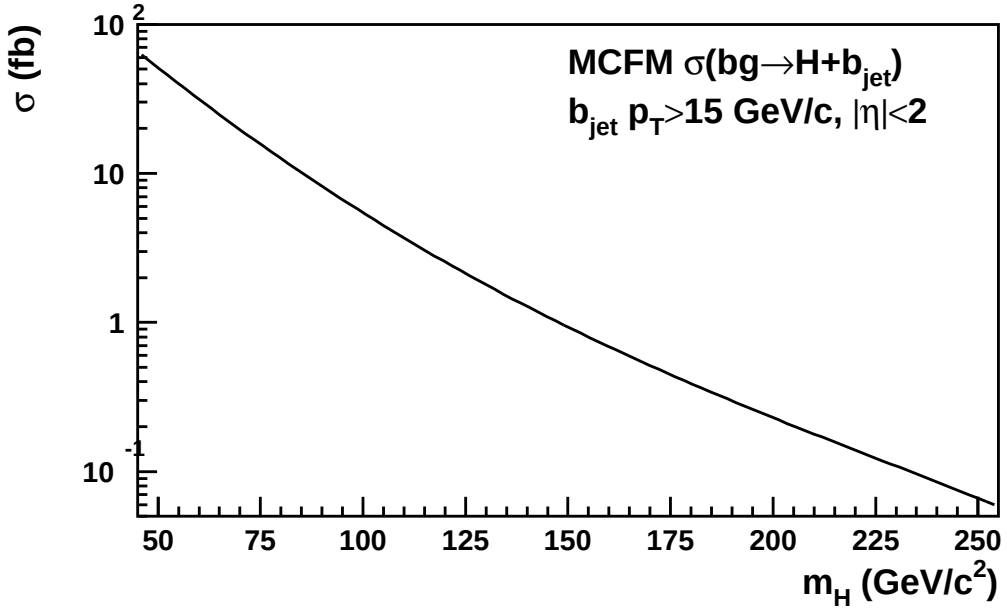

The efficiency of this selection on bH events where the Higgs decays into a $b\bar{b}$ pair is determined from simulated data generated using the PYTHIA [19] Monte Carlo program. The subprocess $gg \to b\bar{b}H$ (`MSUB=121`) is used, with a cut of $p_T > 15$ GeV/c applied to the "beam-side" b quark to reduce generation and simulation time. To more directly match the MCFM cross section calculation at least one associated parton-level b-jet (not b quark) with $p_T > 15$ GeV/c and $|\eta| < 2$ is also required. These b-jets are constructed by running the cone clustering algorithm ($\delta R = 0.4$) on all partons (quarks and gluons) in the event record, after removing those from the Higgs decay, and then choosing only those with a b quark within the jet cone. This requirement rejects events with a hard final state radiation off the b-quark that passed the PYTHIA generation p_T cut. The events are weighted with CTEQ6.5M PDFs, and a small correction is applied to broaden the b_{jet} η distribution to match the MCFM prediction.

The performance of the SECVTX algorithm in the Monte Carlo samples is calibrated to match the data using a procedure similar to that described in Ref. [15], modified to include the effects of the Level2 silicon tracking requirements. The efficiency of the trigger energy cluster matching is also corrected to match the data as a function of the jet E_T. The event selection efficiencies vary from 0.2% to 0.7% as a function of the mass of the Higgs boson and are shown in Figure 6.

The mass of the two leading jets in the event m_{12}, which is used to separate signal from background in our fits, and the SECVTX tag mass combination x_{tags} are shown in Figure 7 for five values of the Higgs mass. For intermediate mass points we derive distributions by histogram interpolation and estimate the selection efficiency using the parametrization shown in Figure 6.

FIG. 6: Selection efficiency for bH events as a function of the Higgs mass m_H.

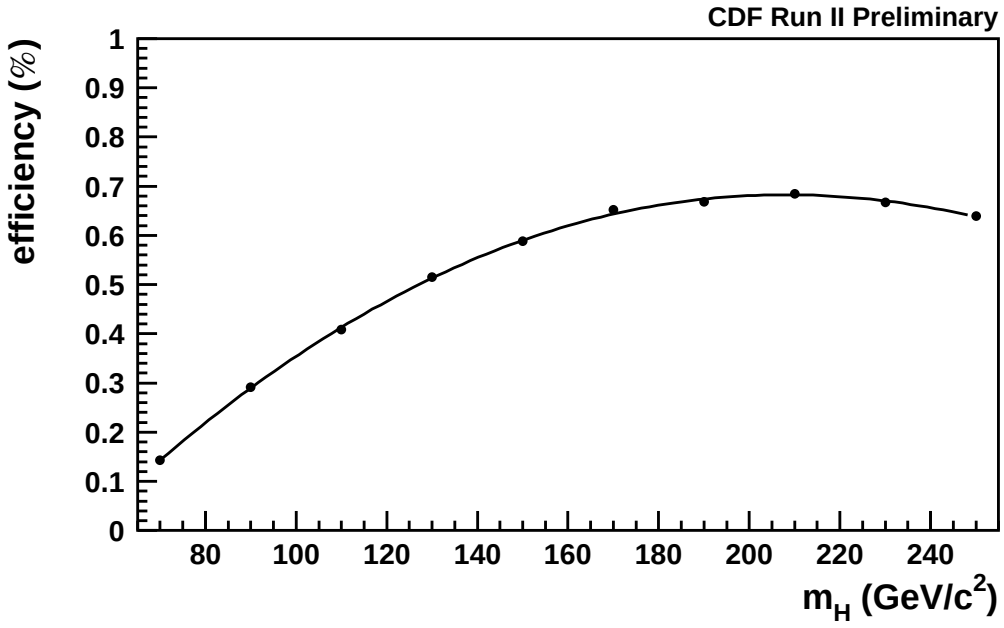

III. BACKGROUNDS

The three-tag sample background is essentially all QCD heavy flavor multijet production. Other processes such as $t\bar{t}$ production and $Z \to b\bar{b}$ + jets were also considered but found to contribute at a negligible level. Using simulated samples of generic QCD multijet production produced with PYTHIA [19] to develop and test our methods, we find that virtually all of the QCD background in our selected triple-tag sample consists of events with at least two real b-tags, with the additional tag being any of a mistagged light jet, a c-tag, or another b-tag. The double-tagged three jet events are found to be predominantly two real b-tags, which makes them a natural starting point for constructing background estimates.

We describe the flavor structure of the jets in the event in the form XXY, where XX is the flavor of the two leading jets (i.e. bq would mean a b-jet (b) and a mistagged light quark (or gluon) jet (q)), while Y is the flavor of the third-leading jet. We make no distinction between the leading and second-leading jets, so that in a bcb event the charm tag could be either of the two leading jets. Under this convention we identify five types of event with at least two real b-tags. Three involve b-tags on both of the leading jets: bbb, bbc, and bbq. The other two, bcb and bqb, have the non-b-tag in one of the two leading jets. The templates we use in our fits for each of these components are shown in Figure 8. Descriptions of our methods for producing these templates follow.

FIG. 7: Distributions of m_{12} (top) and x_{tags} (bottom) for the Higgs signal samples, binned in the indicated increments. The lines simply connect the bin centers and do not represent parametrizations. All are normalized to unit area.

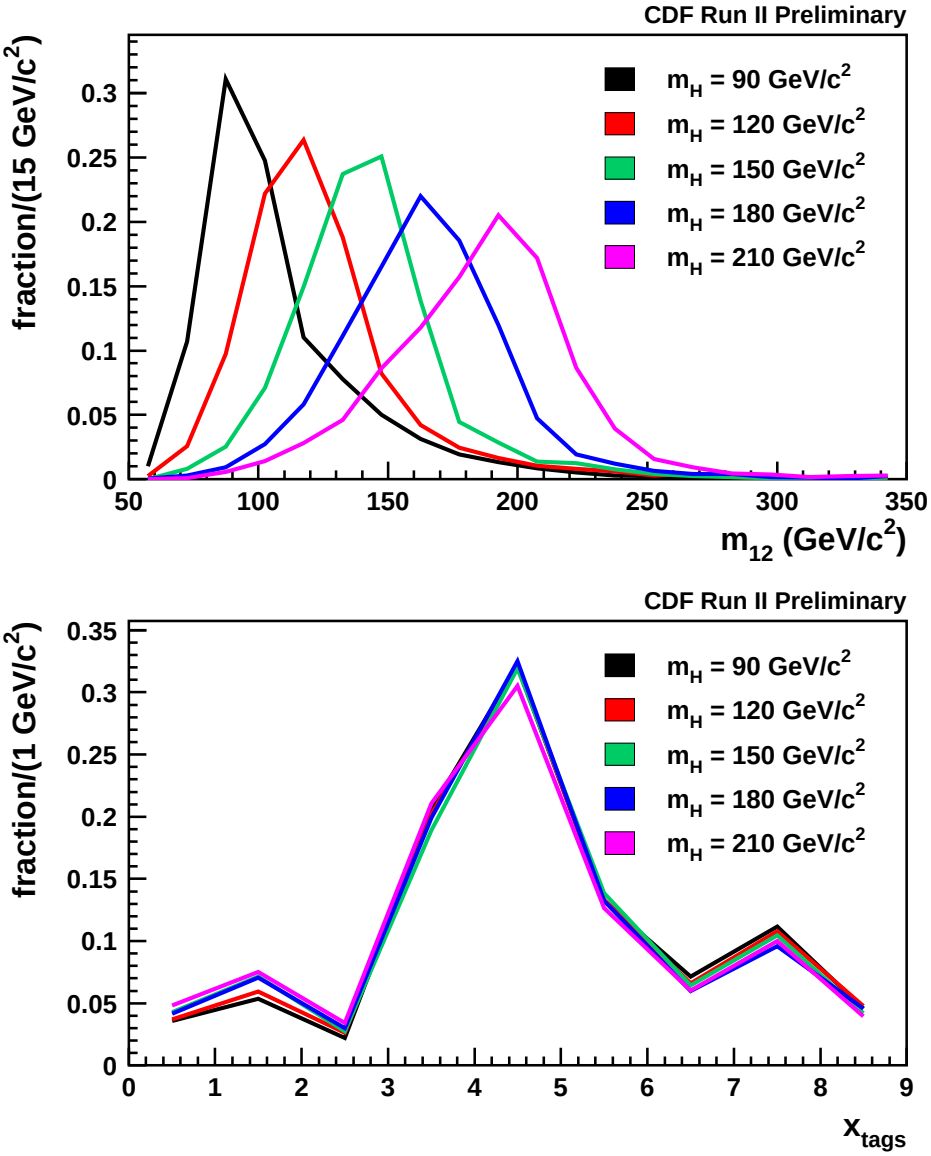

A. General procedure

As noted above, the events with the two leading jets tagged and a third jet are found to largely consist of two real b-tags. This makes them an excellent starting point for constructing estimates of the bbb, bbc, and bbq backgrounds. In order to turn these double-tagged events into estimates of the triple-tagged sample we must simulate the effect of tagging the third jet. This is done using parametrizations of the SECVTX tag efficiency derived from large

FIG. 8: Distributions of m_{12} (top) and x_{tags} (bottom) for the background fit templates, binned in the indicated increments. The lines simply connect the bin centers and do not represent parametrizations. All are normalized to unit area.

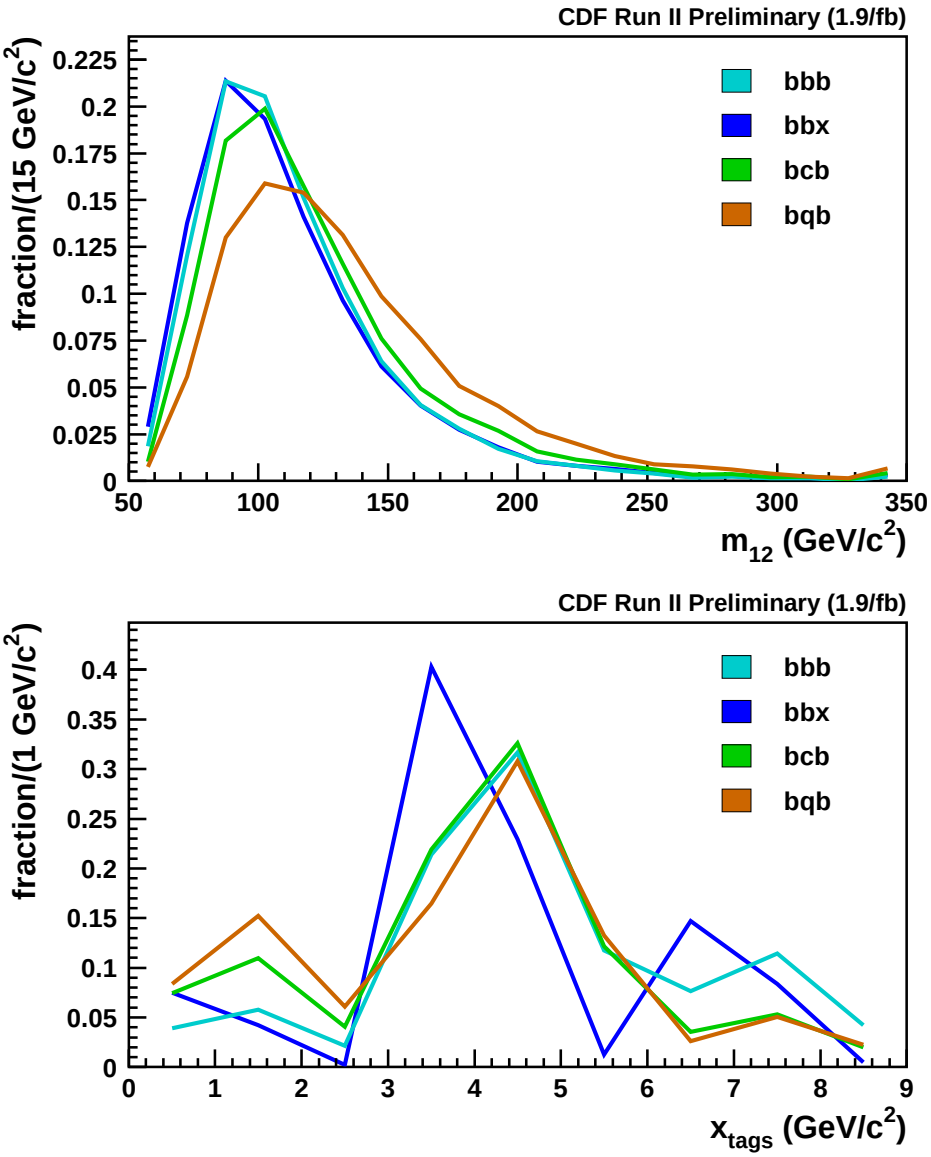

samples of simulated b, c, and light-flavor jets. The tag efficiencies are parametrized as a function of the jet E_T and the number of tracks in the jet passing the SECVTX quality cuts (but with no impact parameter requirement). The parametrizations also give a probability density for the SECVTX tag mass for a jet, defined as the mass of the tracks assigned to the displaced vertex. These tag masses are combined to produce a second discriminating variable alongside m_{12} as described below.

In addition to weighting the events to simulate the third jet tagging, we subtract the component of the double-tagged sample that is not two real b-tags. This is done using events which have two displaced vertices, but where one or both of them are on the opposite side of the primary vertex from the jet direction (negative tags). We weight these events in the same way and then compute

$$N_{b\bar{b}} = N_{++} - \lambda N_{+-} + \lambda^2 N_{--} \tag{2}$$

where N_{++} is the weighted count of observed double-tags in a particular bin of m_{12} and x_{tags}, N_{+-} is the corresponding quantity for events with one of the tags negative, and N_{--} is for both tags negative. The parameter $\lambda = 1.4 \pm 0.2$ reflects the difference between the negative tag rate and the light-flavor fake tag rate, due to the latter including tags from K_S/Λ and interactions with the detector material which will not be present in the negative tags. The effect of this correction on the *bbb* background shape is shown in Figure 9. This correction is applied to all four of the background templates described below.

B. The *bbc* and *bbq* backgrounds

Starting from the corrected double-tagged sample which we call bbj, where j means an untagged third jet, we weight the events by the probability to tag the third jet if it were a c-jet or a light jet to produce estimates for the shapes of the *bbc* and *bbq* background components, respectively. We float these components in an unconstrained fit to the data, so it is not necessary to know how many of the third jets are actually of each flavor, only to get the shapes of the m_{12} and x_{tags} distributions correct. Because there is a positive correlation between all of the jet energies, weighting the third jet as if it were mistagged will bias m_{12} towards higher values than in the *bbc* cases, because the light jet mistag rate rises much more quickly with growing jet E_T than does the c-tag efficiency. This effect can be seen by comparing the *bbc* and *bbq* distributions shown in Figure 8.

C. The *bbb* background

The third-jet weighting procedure works very well for *bbc* and *bbq* backgrounds, because the b-quark production physics is the same as in the bbj events used as the starting point. For the *bbb* background this is not the case. In bbj events there is a contribution from events with a gluon splitting into a $b\bar{b}$ pair, with those two b-jets representing the two leading jets. We find that in these events the two lead jets are less back-to-back than in events where the $b\bar{b}$ are produced directly in the hard scattering process, and therefore have a softer m_{12} distribution. More information on angular correlations in $b\bar{b}$ events and their relation to the various production mechanisms can be found in Ref. [20].

In *bbb* events, PYTHIA indicates that although there is still a sizeable contribution from $b\bar{b}$ pairs produced through gluon splitting, there must be two such splittings in the event and there is no reason why the two lead jets have to come from the same gluon. In fact we find no significant differences in the m_{12} spectra for *bbb* events between the different heavy flavor production mechanisms because of this ability to almost always choose a back-to-back pair. From very large generator-level PYTHIA samples we derive a correction function to map the

FIG. 9: Distributions of m_{12} (top) and x_{tags} (bottom) used to construct the corrected *bbb* background template.

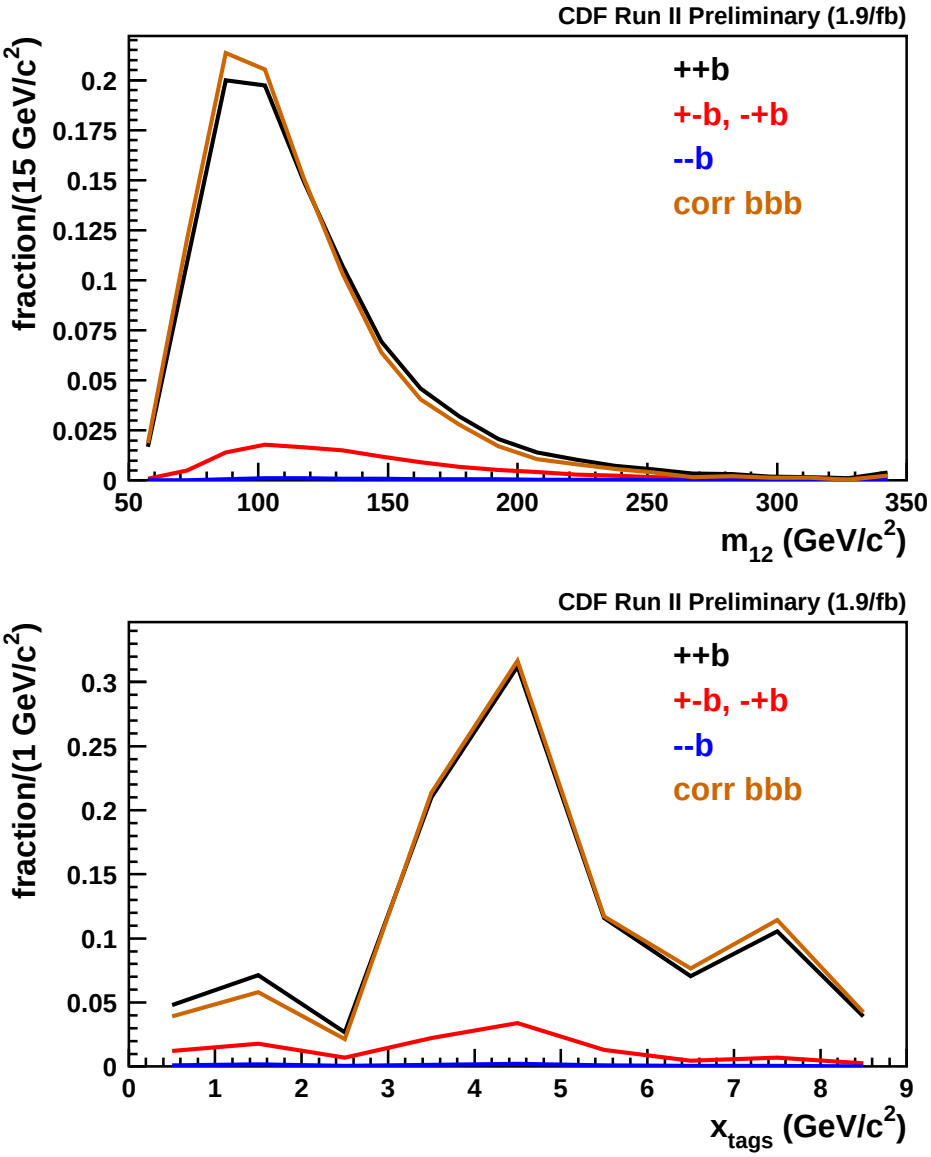

m_{12} distribution of *bbj* events into one appropriate for *bbb*. We calibrate the PYTHIA *bbj* sample to match the results in Table II of Ref. [20] (the "high ISR" row) by scaling up the gluon splitting contribution by a factor of two relative to the other mechanisms. The effect of this correction can be seen by comparing the m_{12} distributions of *bbb* and *bbc* in Figure 8, which would otherwise be essentially identical. Variation of the scale factor applied to the gluon splitting component of *bbj* is the most important systematic error on the background modeling.

D. The *bcb* background

The *bcb* background is similar to *bbb*, with the only difference being the *c*-tag in one of the two leading jets. The charm tag efficiency, while substaintially lower than for *b*-jets, has similar turn-on behavior versus jet E_T and therefore we expect that the m_{12} distribution in our *bbj* sample is a good estimate for what *bcj* would look like (except for the gluon splitting caveat discussed above). Therefore, we only need to correct the SECVTX tag masses of the two leading jets in the *bbj* sample to make a distribution appropriate for *bcj*, using a correction function derived from Monte Carlo simulation. The gluon splitting effect is similar but larger for *bcb* than for *bbb*, because in *bcb* it is explicitly impossible to have the two leading jets come from the same gluon. The effect can be seen in Figure 8, again using *bbc* as a no-correction reference. Neglecting the m_{12} corrections applied to the double-tagged events when forming the *bbb* and *bcb* background templates would bias the Higgs signal fits by greater than the estimated statistical errors, so it is an important effect.

E. The *bqb* background

The last background shape is *bqb*, with two *b*-tags and one mistag that occurs in either of the two leading jets. Ideally we would start from a sample with one *b*-tag and one mistag and weight the third jet as a *b*-tag, however we do not know of a way to select such a sample in the data. Instead, we start from events with a tagged third jet and either of the two leading jets also tagged, and weight using a light jet mistag efficiency parametrization on the untagged jet (also prediciting its SECVTX tag mass). This has the undesirable feature of relying on predictions rather than observed tags in the two lead jets which have much more effect on m_{12} than does the third jet, however we expect this background to be relatively small.

F. Backgrounds summary

The full set of background fit templates is shown in Figure 8. The backgrounds with two heavy flavor tags in the leading jet pair have similar m_{12} distributions, while *bqb* displays a harder spectrum due to the mistag bias. The backgrounds separate into three groups in the x_{tags} view, with *bbc* and *bbq* exhibiting the softest spectra, *bcb* and *bqb* in the middle, and *bbb* (and the Higgs signal) the hardest spectrum. For all background types we do not attempt to predict any absolute normalization. Instead, we float each component in the fit and let the data tell us how much of each type is present in our sample.

IV. SYSTEMATIC UNCERTAINTIES

Several sources of systematic uncertainty on the signal and background contributions are considered. These can take the form of uncertainties on the signal rate, or on the shapes of the fit templates. A summary is shown in Table I. Shape uncertainties are introduced

TABLE I: Summary of systematic uncertainties.

parameter	type	variation	applies to
luminosity	rate	$\pm 6\%$	signal
Monte Carlo statistics	rate	$\pm 2\%$	signal
selection efficiency	rate	$\pm 15\%$	signal
PDFs	rate	$\pm 4\%$	signal
jet energy scale	shape	$\pm 3\%$	signal
SECVTX tag mass modeling	shape	$\pm 3\%$	signal/backgrounds
bbq vs bbc	shape	full range	backgrounds
PYTHIA $g \to b\bar{b}$ rate scale factor	shape	2 ± 1	backgrounds
tag asymmetry factor λ	shape	1.4 ± 0.2	backgrounds

by modifying the templates used when throwing pseudoexperiments using an interpolation procedure, then fitting that modified pseudodata using the original default templates.

Rate uncertainties on the signal contribution relate to the number of events expected for a given cross section. They include the integrated luminosity of the data sample, the statistical errors due to the finite size of the generated signal samples, the efficiency of the trigger and SECVTX tagging requirements, and the effect on the efficiency due to uncertainties on PDFs.

Shape uncertainties are applied to the corrections used for jet energy scale and SECVTX tag mass modeling to match the data. Of these, the jet energy scale is the most significant source of uncertainty, particularly for Higgs masses below 120 GeV/c^2. As can be seen by comparing Figures 7 and 8, there is not a lot of difference between the m_{12} distributions for a low-mass Higgs and the background templates. The signal templates are more sharply peaked, however if the jet energy scale variation in a particular pseudoexperiment is large enough to move the peak in the pseudodata far from the peak in the default fit template, the fit is likely to ascribe many of the signal events in the pseudodata to one of the background templates instead of the signal, reducing the sensitivity. For higher Higgs masses the templates are less sharply peaked and not so similar to the background templates, so the loss in sensitivity is much less severe there.

The background templates float freely in the fit, so only shape uncertainties are considered. The SECVTX tag mass modeling comes in through the parametrizations used to weight the events for the third jet tag bias, which are functions of m_3^{tag}. The bbq and bbc templates are too similar for the fit to constrain them both, so we use an average of the two as our default and interpolate between them to estimate a systematic uncertainty. Varying the value of λ used to subtract the non-$b\bar{b}$ component from the double-tagged events changes the shapes of the resulting corrected background templates but is found not to have a large effect. The uncertainty on the calibration of the gluon splitting rate in PYTHIA applies to the bbb and bcb templates, and is the most important of the sources.

TABLE II: Numbers of fitted events for each background type.

background type	N_{fit}
bbb	1481 ± 165
bbx	512 ± 85
bcb	456 ± 280
bqb	606 ± 170

V. RESULTS

We begin with some simple fits of the data to show how the backgound templates work together. We also perform a fit with a signal template included for illustration. We move on to cross section times branching ratio limits for $bH, H \to b\bar{b}$ production in the case of a narrow standard model-like Higgs. Finally, we interpret our results as limits on $\tan\beta$ in the MSSM as a function of the pseudoscalar Higgs mass m_A, including the effects of the Higgs width.

A. Simple fits of the data

Figure 10 shows the result of a fit of the 3055 triple-tagged events observed in the data using the background templates only and with no systematic errors on the templates. We use a binned maximum-likelihood fit of two-dimensional templates in m_{12} versus x_{tags}; only the projections onto each axis are shown in Figure 10 are shown for clarity. The bbx component is the average of bbq and bbc as discussed in the previous section. The χ^2/dof between the observed data and predicted background is 1.18. The numbers of fitted events for each background type are given in Table II.

A sample fit including a template for a Higgs mass of 150 GeV/c^2 is shown in Figure 11. In this case the χ^2/dof is 1.16, with the fit assigning 50±60 events to the Higgs signal template, with the remaining events distributed among the backgrounds in essentially the same proportions as in Table II.

B. Cross section times branching ratio limits

The limit calculations are performed using the MCLIMIT package [21]. It performs the fitting to either the observed distribution or to pseudoexperiments, and calculates confidence levels using the CL_s method.

Pseudoexperiments are generated using the results of the background-only fit in Figure 10. The background fractions and errors are used to determine how many of each type of event to generate in each pseudoexperiment. The nuisance parameters are set up to reproduce the anticorrelations as closely as possible, so that the total expected number of events in each pseudoexperiment is the same within 20-30 events. For pseudoexperiments that include

FIG. 10: Fit of the triple-tagged data sample using only the QCD background templates, in the m_{12} and x_{tags} projections.

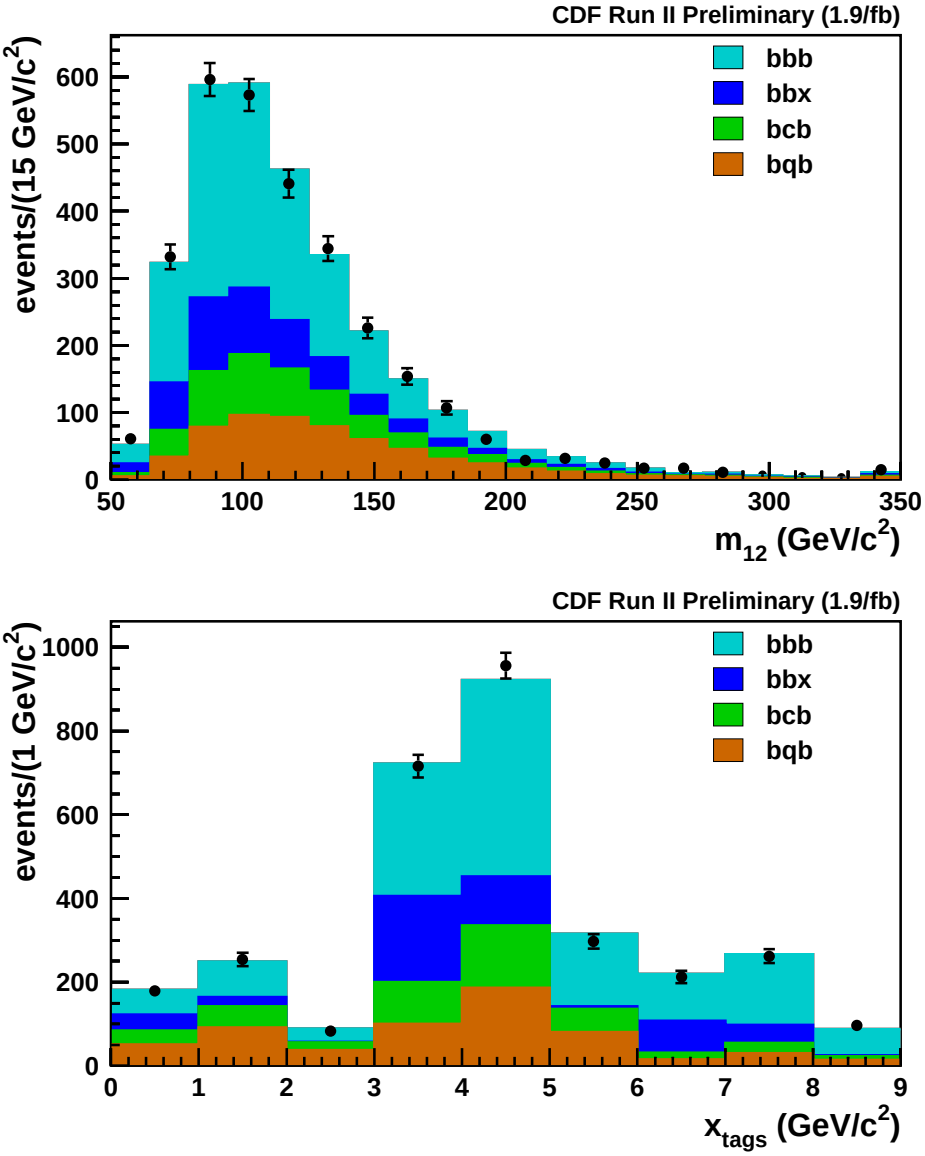

Higgs signal, the expected signal fraction is subtracted from the background fractions in order to keep the average number of events constant.

The median expected limits on $\sigma \times BR$ for statistics only with no systematic errors, with only the variations on the background levels and shapes, and with the full systematics including variations on the signal level and shape are shown in Table III, along with the observed limits. At low Higgs masses there is a considerable loss of senstivity due to systematic errors, primarily due to the jet energy scale and gluon splitting variations as noted above.

FIG. 11: Fit of the triple-tagged data sample using the QCD background templates and one for $m_H = 150$ GeV/c^2.

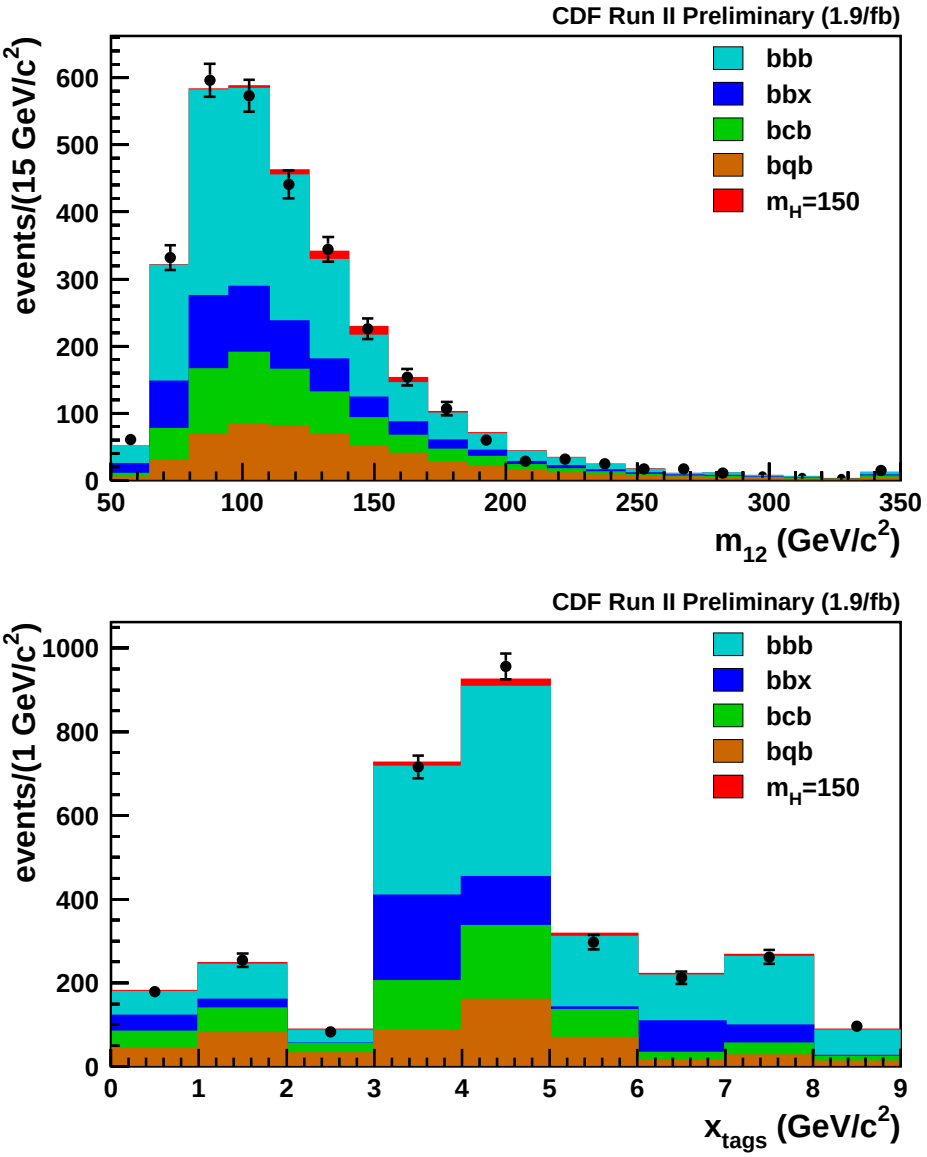

The expected and observed limits for the full systematics case are plotted as a function of the Higgs mass in Figure 12. Also shown are the bands resulting from calculating the expected limits using the $\pm 1\sigma$ and $\pm 2\sigma$ values of the test statistic from background-only pseudoexperiments. No significant deviations from the expected limits are observed.

TABLE III: Median expected and observed limits on $\sigma(p\bar{p} \to bH) \times BR(H \to b\bar{b})$, in pb.

m_H	no systematics	bkgd systematics	full systematics	observed
90	60.4	73.4	76.5	56.7
100	54.4	61.8	108.7	67.2
110	27.4	39.6	49.9	35.4
120	21.6	33.5	41.5	34.6
130	14.5	20.3	23.1	23.3
140	13.7	19.1	21.0	24.2
150	10.6	13.3	15.1	19.1
160	9.8	11.7	12.9	18.8
170	7.4	8.5	9.3	14.3
180	7.2	7.7	8.5	9.5
190	6.0	6.1	6.7	5.5
200	5.6	5.6	6.1	4.1
210	4.7	4.7	5.0	2.9

C. MSSM interpretation

These limits can be trivially converted into limits on $\tan\beta$ versus the pseudoscalar mass m_A in MSSM models by dividing by the standard model cross section times branching ratio (90%), including the factor of two for h/H degeneracy, and taking the square root. The results of this are shown in Figure 13. The limits are not very realistic, however, because they do not include the effects of loop corrections which can enhance the cross section by more or less than $\tan^2\beta$ depending upon the MSSM scenario. They also do not include the effects of the Higgs width which can become significant when the down-type couplings are enhanced by such large factors.

Scaling the SM cross section by $2\tan^2\beta$ is correct at tree level, however loop effects can modify this relationship and introduce dependence on other parameters of the MSSM. In Ref. [1] an approximate expression for the cross section times branching ratio is given as:

$$\sigma(b\bar{b}\phi) \times BR(A \to b\bar{b}) \simeq 2\sigma(b\bar{b}\phi)_{SM} \frac{\tan^2\beta}{(1+\Delta_b)^2} \times \frac{9}{(1+\Delta_b)^2+9} \tag{3}$$

where ϕ is a Higgs boson (either the SM variety or one of $h/H/A$), $\sigma(b\bar{b}\phi)_{SM}$ is the SM cross section, the factor of 2 comes from the degeneracy of A with either h or H, and the loop effects are incorporated into the Δ_b parameter. For our purposes it is important only to note that Δ_b is proportional to the product of $\tan\beta$ and the Higgsino mass parameter μ. Sample values of Δ_b given in Ref. [1] are -0.21 for the m_h^{max} scenario and -0.1 for the no-mixing scenario (at $\mu = -200$ GeV and $\tan\beta = 50$). It is apparent that negative values of μ and hence of Δ_b will increase the MSSM Higgs yield at fixed $\tan\beta$ above the tree level values and result in stronger limits on $\tan\beta$, while scenarios with μ positive will produce the opposite effect. Using Eqn. 3 we can predict the Higgs yield for any value of $\tan\beta$ and Δ_b and therefore derive limits in any desired scenario.

FIG. 12: Median, 1σ, and 2σ expected limits, and observed limits versus m_H on linear (top) and logarithmic (bottom) scales.

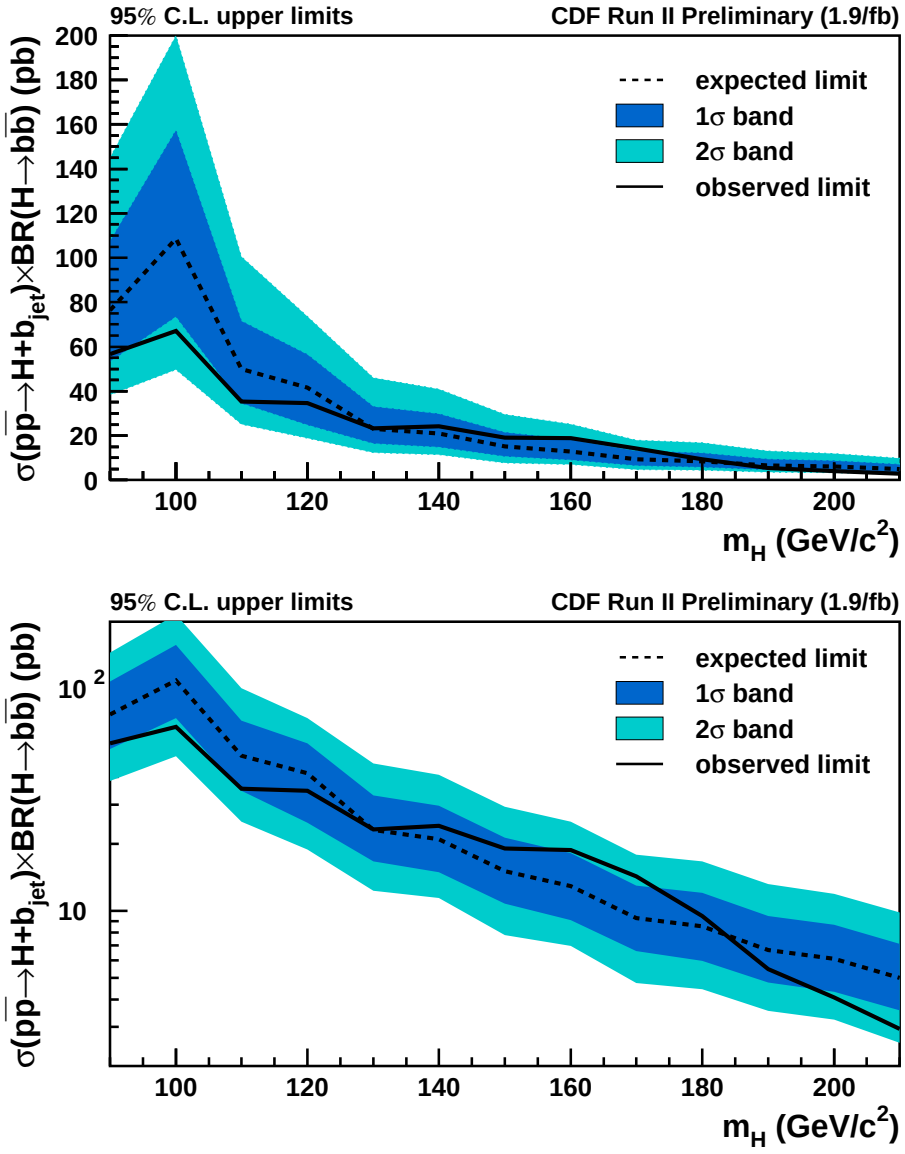

The limits shown in Figures 12 and 13 apply only to narrow Higgs like those in the standard model. If the cross section is increased by scaling the $b\bar{b}H$ coupling, as happens in the MSSM, then the width of the Higgs will increase as well. In order to account for this we convolute the cross section shown in Figure 5 with a relativisitic Breit-Wigner to produce cross section lineshapes for various values of the Higgs pole mass, $\tan\beta$, and Δ_b. Parametrizations of the partial widths $\Gamma_{b\bar{b}}$ and $\Gamma_{\tau\tau}$ as functions of m_A and $\tan\beta$ are obtained from the FEYNHIGGS [22] program, with $\Gamma_{b\bar{b}}$ also dependent on Δ_b.

FIG. 13: Median, 1σ, and 2σ expected $\tan\beta$ limits (not including Higgs width effect or loop corrections), and the observed limits versus m_A.

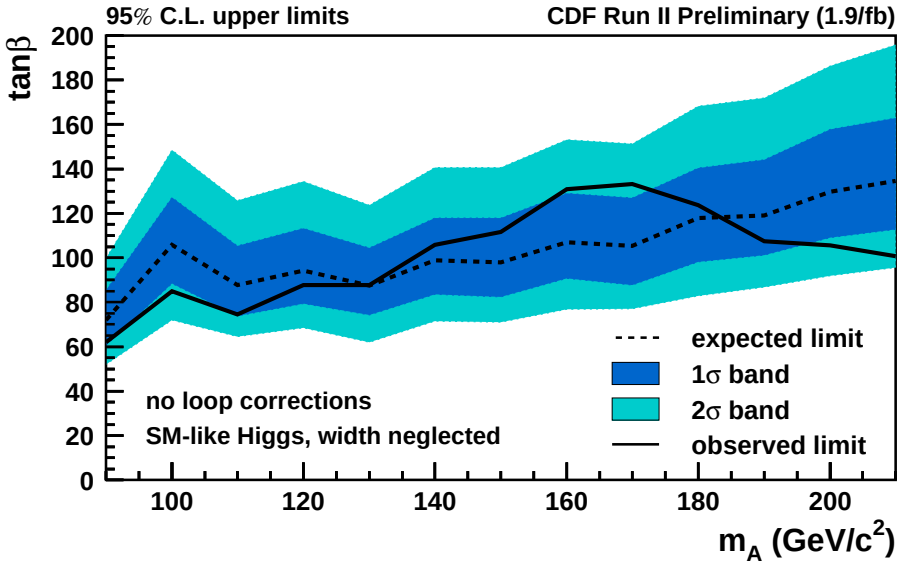

Changing the width of the Higgs also changes the total cross section as a function of the pole mass. We integrate the broadened cross section described above for $m_H > 60$ GeV/c^2 (where the acceptance drops to zero) and divide by the no-width SM value to derive an enhancement factor. This factor ranges from 0.95-0.75 for pole mass of 90 GeV/c^2 to 1.05-1.40 for 180 GeV/c^2, for $\tan\beta$ from 40-150. The factor drops below 1 for low pole mass because of the cutoff at 60 GeV/c^2. This information is needed when computing the expected number of events for a given Higgs mass and $\tan\beta$ value in the limits calculator.

Fit templates as a function of $\tan\beta$ are constructed by combining the narrow-width templates, weighted by the m_H lineshapes and by the acceptance parametrization shown in Figure 6. An example is shown in Figure 14.

We scan in $\tan\beta$ from 40 to 200 in steps of 5 and calculate CL_s at each point, and exclude regions with $CL_s > 0.05$. The limits obtained are shown in Figure 15 for $\Delta_b = 0$. The limits get weaker in a highly $\tan\beta$-dependent way, so that compared with Figure 13 the -2σ contour moves much less than the $+2\sigma$ one does. This is because as $\tan\beta$ increases, the growing width spreads the events out over a larger region of m_{12}, reducing the fit power, and also tends to reduce the number of expected events due to the cross section lineshape extending downwards into regions with low or no acceptance. Below 100 GeV/c^2 we find little sensitivity after including the Higgs width and do not report limits there.

To illustrate why the limits worsen so quickly at high $\tan\beta$, Figure 16 shows the result of a simple fit of the data similar to what is shown in Figure 11, except the signal template includes the width effects. As shown in Figure 14, the net effect is for the signal to spread out into more bins, and also to shift towards lower values of m_{12} where the backgrounds are larger. Both of these effects reduce the statistical sensitivity of the search and require

FIG. 14: Distributions of m_{12} for varying $\tan\beta$ and $\Delta_b = 0$, for Higgs pole mass of 150 GeV/c^2. The normalizations indicate the acceptance relative to the SM case which has unit area.

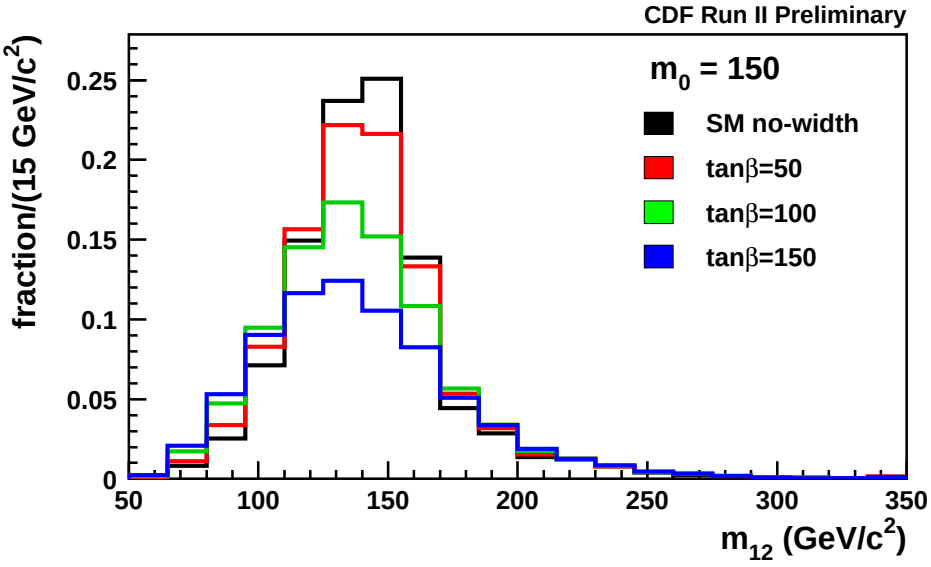

FIG. 15: Median, 1σ, and 2σ expected limits, and the observed limits versus m_A, including the Higgs width and for $\Delta_b = 0$.

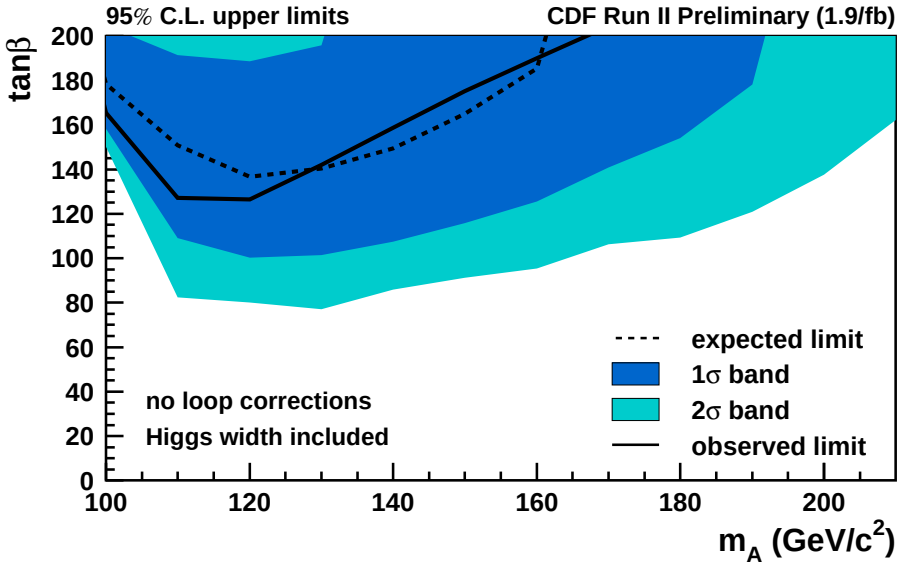

FIG. 16: Fit of the triple-tagged data sample using the QCD background templates and one for $m_H = 150$ GeV/c^2 with $\tan\beta = 100$ and $\Delta_b = 0$. Only the m_{12} projection is shown.

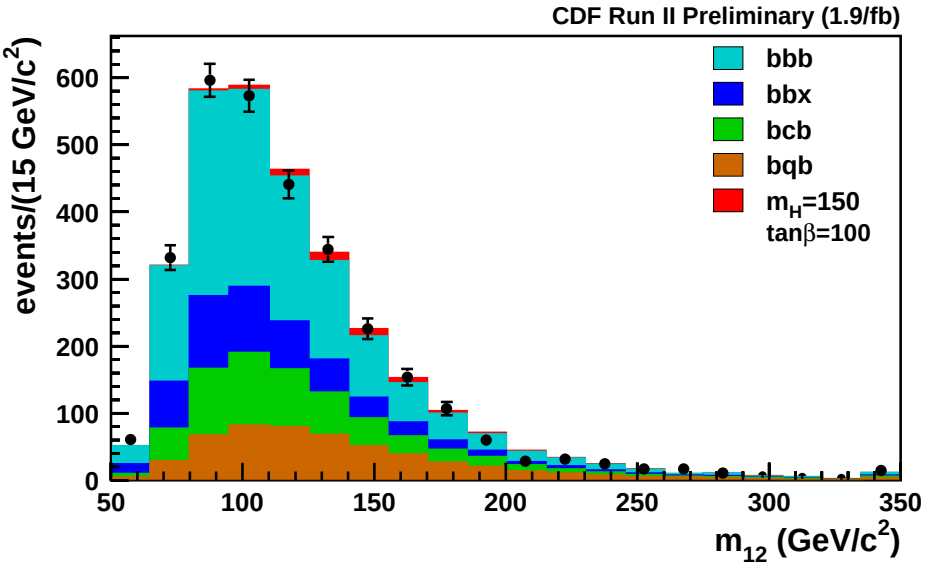

adding more signal to reach CL_s of 0.05, however that additional signal (i.e. higher $\tan\beta$) further broadens and shifts the m_{12} distribution, and so on.

Along with the $\Delta_b = 0$ case, limits are also generated for the m_h^{max} scenario with $\mu = -200$ GeV and are shown in Figure 17. Because of the relatively large and negative values of Δ_b in this scenario, the $\tan\beta$ limits are much tighter.

VI. CONCLUSION

A search for Higgs bosons produced in association with b-quarks was performed in 1.9 fb^{-1} of data. This process could be visible in supersymmetric models with high values of $\tan\beta$. The variable used was the mass of the two leading jets in triple-tagged events, with additional information from the SECVTX tag masses included to improve the background modeling.

The observed limits are within 2σ of expectations over the mass region from 90 to 210 GeV/c^2, with the largest excess occuring around 160 GeV/c^2. The results are interpreted in two MSSM scenarios. In the case where loop effects are small, we find that the growth of the Higgs width as the couplings are enhanced permits only weak limits on $\tan\beta$. In the m_h^{max} scenario with μ negative, the enhanced production through loop effects allows exclusion of $\tan\beta$ values greater than 80-120 over the mass range 90-190 GeV/c^2.

FIG. 17: Median, 1σ, and 2σ expected limits, and the observed limits versus m_H, including the Higgs width, for the m_h^{max} scenario with $\mu = -200$ GeV.

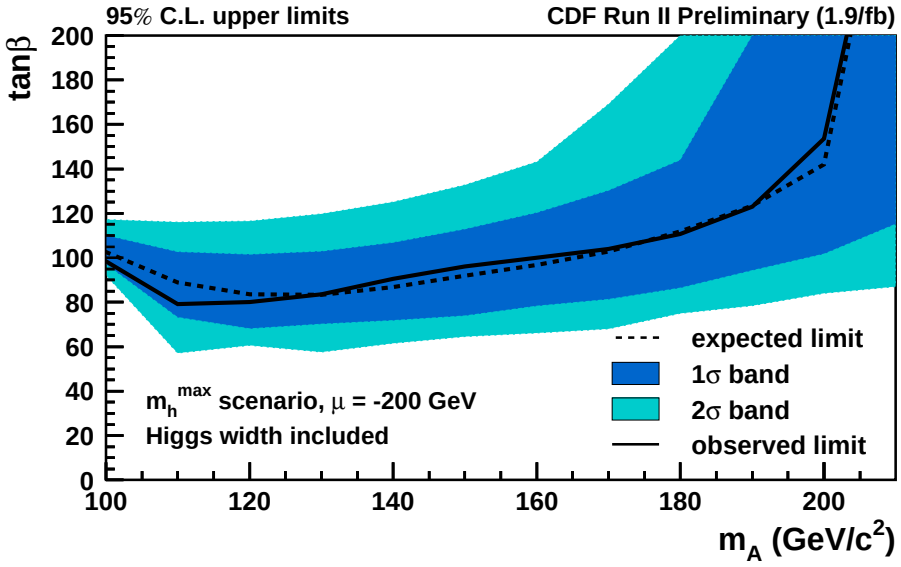

Acknowledgments

We thank the Fermilab staff and the technical staffs of the participating institutions for their vital contributions. This work was supported by the U.S. Department of Energy and National Science Foundation; the Italian Istituto Nazionale di Fisica Nucleare; the Ministry of Education, Culture, Sports, Science and Technology of Japan; the Natural Sciences and Engineering Research Council of Canada; the National Science Council of the Republic of China; the Swiss National Science Foundation; the A.P. Sloan Foundation; the Bundesministerium für Bildung und Forschung, Germany; the Korean Science and Engineering Foundation and the Korean Research Foundation; the Science and Technology Facilities Council and the Royal Society, UK; the Institut National de Physique Nucleaire et Physique des Particules/CNRS; the Russian Foundation for Basic Research; the Comisión Interministerial de Ciencia y Tecnología, Spain; the European Community's Human Potential Programme; the Slovak R&D Agency; and the Academy of Finland.

[1] M. Carena, S. Heinemeyer, C. E. M. Wagner, and G. Weiglein, "MSSM Higgs boson searches at the Tevatron and the LHC: Impact of different benchmark scenarios," *Eur. Phys. J.* **C45** (2006) 797–814, `hep-ph/0511023`.

[2] F. Maltoni. `http://maltoni.home.cern.ch/maltoni/TeV4LHC/`.

[3] R. V. Harlander and W. B. Kilgore, "Higgs boson production in bottom quark fusion at next-to- next-to-leading order," *Phys. Rev.* **D68** (2003) 013001, `hep-ph/0304035`.

[4] S. Dawson, C. B. Jackson, L. Reina, and D. Wackeroth, "Higgs production in association with bottom quarks at hadron colliders," hep-ph/0508293.

[5] S. Dawson, C. B. Jackson, L. Reina, and D. Wackeroth, "Hadronic Higgs production with heavy quarks at the Tevatron and the LHC," hep-ph/0603112.

[6] J. Campbell, R. K. Ellis, F. Maltoni, and S. Willenbrock, "Higgs boson production in association with a single bottom quark," *Phys. Rev.* **D67** (2003) 095002, hep-ph/0204093.

[7] J. Campbell *et al.*, "Higgs boson production in association with bottom quarks," hep-ph/0405302.

[8] **DØ** Collaboration, V. M. Abazov *et al.*, "Search for neutral supersymmetric Higgs bosons in multijet events at $\sqrt{s} = 1.96$ TeV," *Phys. Rev. Lett.* **95** (2005) 151801, hep-ex/0504018.

[9] **DØ** Collaboration, "Search for Neutral Higgs Bosons at high $\tan\beta$ in Multijet Events," D0Note 5503-CONF. http://www-d0.fnal.gov/Run2Physics/WWW/results/prelim/HIGGS/H23/H23.pdf.

[10] **CDF** Collaboration, A. Abulencia *et al.*, "Search for neutral MSSM Higgs bosons decaying to tau pairs in $p\bar{p}$ collisions at $\sqrt{s} = 1.96$ TeV," *Phys. Rev. Lett.* **96** (2006) 011802, hep-ex/0508051.

[11] **CDF** Collaboration, "Search for Neutral MSSM Higgs Boson(s) Decaying to Tau Pairs with 1.8/fb of Data," CDF Note 9071. http://www-cdf.fnal.gov/physics/new/hdg/results/htt_070928/note/cdf9071.pdf.

[12] **DØ** Collaboration, V. M. Abazov *et al.*, "Search for neutral Higgs bosons decaying to τ pairs in $p\bar{p}$ collisions at $\sqrt{s} = 1.96$ TeV," *Phys. Rev. Lett.* **97** (2006) 121802, hep-ex/0605009.

[13] **DØ** Collaboration, "Search for Neutral Higgs Boson Production in the Decay $h \to \tau_\mu \tau$ with the DØDetector at $\sqrt{s} = 1.96$ TeV," DØNote 5331-CONF. http://www-d0.fnal.gov/Run2Physics/WWW/results/prelim/HIGGS/H29/H29.pdf.

[14] **DØ** Collaboration, "Search for Neutral Higgs Bosons at high $\tan\beta$ in the $b(h/H/A) \to b\tau\tau$ Channel," DØNote XXXX-CONF. http://www-d0.fnal.gov/Run2Physics/WWW/results/prelim/HIGGS/H24/H24.pdf.

[15] **CDF** Collaboration, "Measurement of the $t\bar{t}$ production cross section in $p\bar{p}$ collisions at $\sqrt{s} = 1.96$ TeV using Lepton+Jets Events with Secondary Vertex b-Tagging," CDF Note 8795. http://www-cdf.fnal.gov/physics/new/top/confNotes/cdf8795_SecVtxXSPublic.ps.

[16] **CDF** Collaboration, D. Acosta *et al.*, "Measurement of the J/ψ meson and $b-$hadron production cross sections in $p\bar{p}$ collisions at $\sqrt{s} = 1960$ GeV," *Phys. Rev.* **D71** (2005) 032001, hep-ex/0412071.

[17] W. K. Tung *et al.*, "Heavy quark mass effects in deep inelastic scattering and global QCD analysis," *JHEP* **02** (2007) 053, hep-ph/0611254.

[18] F. Maltoni, Z. Sullivan, and S. Willenbrock, "Higgs-boson production via bottom-quark fusion," *Phys. Rev.* **D67** (2003) 093005, hep-ph/0301033.

[19] T. Sjostrand, S. Mrenna, and P. Skands, "PYTHIA 6.4 physics and manual," *JHEP* **05** (2006) 026, hep-ph/0603175.

[20] **CDF** Collaboration, D. Acosta *et al.*, "Measurements of $b\bar{b}$ azimuthal production correlations in $p\bar{p}$ collisions at $\sqrt{s} = 1.8$ TeV," *Phys. Rev.* **D71** (2005) 092001, hep-ex/0412006.

[21] T. Junk and J. Heinrich. https://plone4.fnal.gov:4430/P0/phystat/packages/0711001.

[22] S. Heinemeyer *et al.* http://www.feynhiggs.de/.